Impact of Ferromagnetic Yokes on Axial Flux Passively Levitated Self-Bearing Machines

1st Joachim Van Verdeghem, 2nd Adrien Robert, 3rd Simon Herrman, 4th Bruno Dehez
Division of Mechatronic, Electrical Energy and Dynamic Systems (MEED),
Université catholique de Louvain (UCLouvain)
Louvain-La-Neuve, Belgium
joachim.vanverdeghem@uclouvain.be

***Abstract*—Self-bearing machines have gained increasing interest over the past twenty years by bringing the benefits of magnetic suspension to high torque density systems. Among them, passively levitated machines have recently been investigated both at the theoretical and experimental levels, being nevertheless limited to ironless structures for the axial flux configuration. In this context, this paper introduces a rotor structure comprising a ferromagnetic yoke surrounding the armature winding. The scope of the existing electromechanical model is then enlarged to take into consideration the resulting variation of the inductance coefficients with the rotor axial position. Additional force and torque terms created by the motor current are highlighted. Finally, the proposed structure is compared to the classical ironless rotor, underlining that the former allows to increase the motor and suspension performance metrics.**

***Index Terms*—Self-bearing, bearingless, electromechanical model, reluctant force, inductance variation**

I. Introduction

Self-bearing machines offer an attractive solution for magnetically suspended systems requiring a high torque density or a short rotor length [1]. Benefiting from the advantages of magnetic levitation, namely the absence of wear and lubrication, these machines are implemented in applications such as reaction wheel and flywheels [2], [3], blowers and fans [4], [5], hygienic pump and mixing devices [6], [7] as well as ventricular assist devices [8], [9] but also in significant power industrial and transportation applications [10]. Among these machines, passively levitated structures relying on electrodynamic forces have been investigated to further increase the compactness, improve the reliability and reduce the overall cost by removing the position sensors and the electronics dedicated to the rotor suspension [11]. Analytical electromechanical models allowing to predict the rotor dynamics of both axial and radial flux implementations of these machines have been established and extensively validated through experimental characterizations [11]–[15]. However, unlike their radial flux counterparts and in particular the bell-shaped configuration analysed in [15], the axial flux structures studied so far do not include rotor ferromagnetic yokes behind the armature winding while this

This work is funded by the Walloon Region (Belgium), SPW-Economie Emploi Recherche through the Win2Wal program, convention #2010131.

978-1-6654-9302-4/22/$31.00

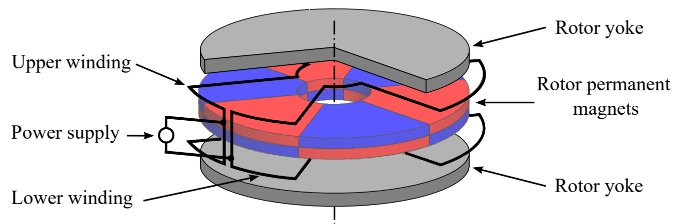

Fig. 1. Axial flux passively levitated self-bearing machine including additional rotor ferromagnetic yokes (with $p = 3$ and only one phase represented).

may offer several advantages such as limited stray fields, increased inductance coefficients and airgap flux density as well as potential additional force components.

In this context, this paper first introduces a novel rotor structure comprising a ferromagnetic yoke surrounding the armature winding. The existing electromechanical model is then generalised to take into account the impact of the inductance coefficient variation with the rotor axial position on the electrical equations and the electromagnetic forces. The motor and suspension performance of the proposed structure are finally studied and compared to the classical ironless machine in the framework of a case study.

II. Structure

The proposed self-bearing machine structure is shown in Fig. 1. The stator includes two identical three-phase windings connected in parallel to the power supply. The rotor relies on a permanent magnet arrangement located between both windings and creating a p pole-pair axial magnetic field. Compared to the classical ironless implementation, the rotor also encompasses two ferromagnetic yokes placed on both machine sides behind the windings. At the expense of an increased manufacturing complexity, this structure allows to enclose the magnetic field within the machine, thereby limiting stray fields. In addition, the axial component of the magnetic flux density is strengthened in the airgap, improving the drive torque, but its axial variation is reduced, affecting the suspension force that depends on the gradient of the permanent magnet flux linked by the windings [11]. The inductance coefficients are also increased, lowering the electrical pole and thus implying that the asymptotic axial restoring force is reached at lower spin speeds.

III. Electromechanical Model

This section extends the electromechanical model derived in [11] by taking into account the axial variation of the inductance coefficients resulting, in this instance, from the additional rotor yokes placed on both sides of the machine.

A. PM flux linkage

Assuming small rotor axial displacements, the permanent magnet fluxes linked by the upper and lower windings, denoted $\mathbf{\Phi_U}$ and $\mathbf{\Phi_L}$ respectively, can be linearised, yielding:

$$\begin{aligned} \mathbf{\Phi_U} &= (K_\alpha + zK_z)\cos(p\alpha - \boldsymbol{\delta}) \\ \mathbf{\Phi_L} &= (K_\alpha - zK_z)\cos(p\alpha - \boldsymbol{\delta}) \end{aligned}, \tag{1}$$

where $\boldsymbol{\delta} = [0,\ 2\pi/3,\ 4\pi/3]^{\mathrm{T}}$ is a vector including the angular position of the three phases, α is the rotor spin position, K_α is the flux constant, namely the amplitude of the flux linkage in the centred position, and K_z is the flux gradient, i.e. the proportionality factor between the flux amplitude and the rotor axial position z.

B. Inductance Coefficients

Under the hypothesis of small rotor axial displacements, the upper and lower inductance coefficients, referred to as $\mathbf{L_U}$ and $\mathbf{L_L}$, can be written as follows:

$$\begin{aligned} \mathbf{L_U}(z) &= \mathbf{L} + z\mathbf{L_z} \\ \mathbf{L_L}(z) &= \mathbf{L} - z\mathbf{L_z} \end{aligned}, \tag{2}$$

with:

$$\mathbf{L} = \begin{pmatrix} L & L_m & L_m \\ L_m & L & L_m \\ L_m & L_m & L \end{pmatrix},\ \mathbf{L_z} = \begin{pmatrix} L_z & L_{z,m} & L_{z,m} \\ L_{z,m} & L_z & L_{z,m} \\ L_{z,m} & L_{z,m} & L_z \end{pmatrix} \tag{3}$$

where $\mathbf{L}$ includes the self and mutual inductance coefficients of the upper/lower phase windings, denoted L and L_m, in the centred position while $\mathbf{L_z}$ encompasses their respective variations L_z and $L_{z,m}$ with the rotor axial position z. Note that, for the structure under study, the upper inductance coefficient $\mathbf{L_U}$ reduces for a positive axial displacement z while the lower one $\mathbf{L_L}$ increases and conversely for negative displacements, implying that $\mathbf{L_z}$ is negative.

In contrast, assuming small displacements and thereby neglecting second and higher order terms, the mutual inductance coefficients $\mathbf{M}$ between the upper and lower phase windings do not depend on the rotor position z thanks to the axial symmetry of the considered machine:

$$\mathbf{M} = \begin{pmatrix} M & M_m & M_m \\ M_m & M & M_m \\ M_m & M_m & M \end{pmatrix}. \tag{4}$$

C. Electrical Equations

Considering the independence of the mutual inductance coefficient with respect to the axial position and thus to time, the electrical equations governing the evolution of the upper and lower winding currents, denoted $\mathbf{i_U}$ and $\mathbf{i_L}$, reduce to:

$$\begin{aligned} \mathbf{u} &= R\mathbf{i_U} + \mathbf{L_U}\frac{d\mathbf{i_U}}{dt} + \frac{d\mathbf{L_U}}{dt}\mathbf{i_U} + \mathbf{M}\frac{d\mathbf{i_L}}{dt} + \frac{d\mathbf{\Phi_U}}{dt} \\ \mathbf{u} &= R\mathbf{i_L} + \mathbf{L_L}\frac{d\mathbf{i_L}}{dt} + \frac{d\mathbf{L_L}}{dt}\mathbf{i_L} + \mathbf{M}\frac{d\mathbf{i_U}}{dt} + \frac{d\mathbf{\Phi_L}}{dt} \end{aligned} \tag{5}$$

where $\mathbf{u}$ is the three-phase voltage applied to the armature and R is the phase winding resistance. As demonstrated in [11], the upper and lower winding currents can be seen as the superposition of the classic motor current $\mathbf{i_M}$, provided by the power supply, and a suspension current $\mathbf{i_S}$, induced in the windings in case of rotor decentring, defined as:

$$\begin{aligned} \mathbf{i_M} &= \mathbf{i_U} + \mathbf{i_L} \\ \mathbf{i_S} &= \frac{\mathbf{i_U} - \mathbf{i_L}}{2} \end{aligned} \tag{6}$$

Substituting (6) into (5) leads to:

$$\begin{aligned} \mathbf{u} &= \frac{R}{2}\mathbf{i_M} + \left(\frac{\mathbf{L}+\mathbf{M}}{2}\right)\frac{d\mathbf{i_M}}{dt} + K_\alpha\frac{d[\cos(p\alpha - \boldsymbol{\delta})]}{dt} \\ &\quad + z\mathbf{L_z}\frac{d\mathbf{i_S}}{dt} + \frac{dz}{dt}\mathbf{L_z}\mathbf{i_S} \\ 0 &= 2R\mathbf{i_S} + 2(\mathbf{L}-\mathbf{M})\frac{d\mathbf{i_S}}{dt} + 2K_z\frac{d[z\cos(p\alpha - \boldsymbol{\delta})]}{dt} \\ &\quad + z\mathbf{L_z}\frac{d\mathbf{i_M}}{dt} + \frac{dz}{dt}\mathbf{L_z}\mathbf{i_M} \end{aligned} \tag{7}$$

Omitting initially the additional terms resulting from the inductance coefficient variation $\mathbf{L_z}$, the first set of equations governs the motor function, the latter operating based on the motor current $\mathbf{i_M}$ flowing in the upper and lower windings connected in parallel to the power supply $\mathbf{u}$. The second set is related to the rotor axial suspension that relies on the suspension current $\mathbf{i_S}$ circulating in the short-circuited path formed by windings in series. As soon as the rotor is decentred or moves axially, the additional terms create a coupling between the motor and suspension equations. This coupling generates a disturbance on the motor operation but might be beneficial for the rotor magnetic suspension, as will be discussed hereinafter. The machine electrical equations can be further developed by applying the Park-Concordia transformation:

$$\begin{aligned} u_d &= \frac{R}{2}i_{M,d} + \frac{L_c + M_c}{2}(\dot{i_{M,d}} - p\omega i_{M,q}) \\ &\quad + L_{z,c}(\dot{z}i_{S,d} + z\dot{i_{S,d}} - p\omega z i_{S,q}) \\ u_q &= \frac{R}{2}i_{M,q} + \frac{L_c + M_c}{2}(\dot{i_{M,q}} + p\omega i_{M,d}) \\ &\quad + L_{z,c}(\dot{z}i_{S,q} + z\dot{i_{S,q}} + p\omega z i_{S,d}) + p\omega K_\alpha\sqrt{3/2} \\ 0 &= 2Ri_{S,d} + 2(L_c - M_c)(\dot{i_{S,d}} - p\omega i_{S,q}) \\ &\quad + L_{z,c}(\dot{z}i_{M,d} + z\dot{i_{M,d}} - p\omega z i_{M,q}) + 2\dot{z}K_z\sqrt{3/2} \\ 0 &= 2Ri_{S,q} + 2(L_c - M_c)(\dot{i_{S,q}} + p\omega i_{S,d}) \\ &\quad + L_{z,c}(\dot{z}i_{M,q} + z\dot{i_{M,q}} + p\omega z i_{M,d}) + 2p\omega z K_z\sqrt{3/2} \end{aligned} \tag{8}$$

where $L_c = L - L_m$, $M_c = M - M_m$ and $L_{z,c} = L_z - L_{z,m}$ are the self, mutual and variational synchronous inductance coefficients. The additional electromotive forces induced in the equations related to the axial levitation by the direct-axis motor current $i_{M,d}$, that does not participate in the force and torque creation in classical machines such as the ironless structure, opens up the possibility to modulate the suspension current and thus the axial force when the rotor is decentred.

D. Electromagnetic Forces

The electromagnetic force is derived following the magnetic coenergy approach and can be separated into two contributions, namely the electrodynamic and reluctant forces.

1) Electrodynamic Forces: The electrodynamic force $F_{z,e}$, that arises from the interaction between the permanent flux linked by the upper and lower windings and currents flowing within them, can be expressed based on the motor and suspension currents as follows:

$$\begin{aligned}F_{z,e} &= \left[\frac{d\mathbf{\Phi_U}}{dz}\right]^{\mathrm{T}} \mathbf{i_U} + \left[\frac{d\mathbf{\Phi_L}}{dz}\right]^{\mathrm{T}} \mathbf{i_L} \\ &= \left[\frac{d\mathbf{\Phi_S}}{dz}\right]^{\mathrm{T}} \mathbf{i_S} + \underbrace{\left[\frac{d\mathbf{\Phi_M}}{dz}\right]^{\mathrm{T}}}_{=0} \mathbf{i_M} \\ &= 2K_z\sqrt{\frac{3}{2}}i_{S,d}.\end{aligned} \tag{9}$$

Similarly, the electrodynamic torque $T_{\alpha,e}$ is calculated as:

$$\begin{aligned}T_{\alpha,e} &= \left[\frac{d\mathbf{\Phi_U}}{d\alpha}\right]^{\mathrm{T}} \mathbf{i_U} + \left[\frac{d\mathbf{\Phi_L}}{d\alpha}\right]^{\mathrm{T}} \mathbf{i_L} \\ &= \left[\frac{d\mathbf{\Phi_S}}{d\alpha}\right]^{\mathrm{T}} \mathbf{i_S} + \left[\frac{d\mathbf{\Phi_M}}{d\alpha}\right]^{\mathrm{T}} \mathbf{i_M} \\ &= \underbrace{zp2K_z\sqrt{\frac{3}{2}}i_{S,q}}_{T^S_{\alpha,e}} + \underbrace{pK_\alpha\sqrt{\frac{3}{2}}i_{M,q}}_{T^M_{\alpha,e}}.\end{aligned} \tag{10}$$

These expressions are identical to that obtained for the classical ironless structure [11]. Specifically, the motor torque $T^M_{\alpha,e}$ is only produced through the quadrature-axis motor current $i_{M,q}$. On the other hand, the restoring force $F_{z,e}$ and the drag torque $T^S_{\alpha,e}$, that counteracts the drive torque, are respectively created by the direct and quadrature components of the suspension current. It is important to remember that this current solely results from the electromotive forces induced in the windings since the suspension equations do not involve the power supply. However, although their expressions in (9) and (10) have no direct dependence to the motor current, the latter does impact the axial electrodynamic force an drag torque through the coupling terms resulting from the axial variation of the inductance coefficients, as highlighted in the suspension electrical equations in (8) and further investigated under quasi-static conditions in Section III-E.

2) Reluctant Forces: The reluctant force $F_{z,r}$, that results from the variation of the inductance coefficient with the rotor axial position, can written as:

$$F_{z,r} = \frac{1}{2}\left(\mathbf{i_U}^{\mathrm{T}}\frac{d\mathbf{L_U}}{dz}\mathbf{i_U} + \mathbf{i_L}^{\mathrm{T}}\frac{d\mathbf{L_L}}{dz}\mathbf{i_L} + \mathbf{i_U}^{\mathrm{T}}\frac{d\mathbf{M}}{dz}\mathbf{i_L}\right). \tag{11}$$

Recalling that the mutual inductance coefficient $\mathbf{M}$ between the upper and lower windings is independent from the axial position z and substituting (6) into (11) to express the force in terms of the motor and suspension currents yields:

$$F_{z,r} = \mathbf{i_M}^{\mathrm{T}}\mathbf{L_z}\mathbf{i_S}. \tag{12}$$

This force can be expressed in the Park reference frame as:

$$F_{z,r} = L_{z,c}(i_{M,d}\,i_{S,d} + i_{M,q}\,i_{S,q}). \tag{13}$$

This expression depends on the product between the motor and suspension currents, implying that no reluctant force can be generated when the rotor is axially centred in steady state.

In contrast, there is no reluctant torque since the inductance coefficients $\mathbf{L_U}$, $\mathbf{L_L}$ and $\mathbf{M}$ do not vary with the spin position α because of the axisymmetric rotor magnetic circuit.

E. Quasi-static Analysis

The quasi-static analysis, carried out assuming fixed rotor position z and spin speed ω, provides a valuable insight on the machine behaviour by investigating the electrical currents and the resulting force and torque in steady-state. Considering that the motor current is controlled, the direct and quadrature-axis components of the suspension current in quasi-static conditions can be retrieved from (8), yielding:

$$\begin{aligned}i_{S,d} &= z\frac{\omega}{\omega^2+\left(\frac{1}{p}\frac{R}{L_{S,c}}\right)^2}\frac{1}{2}\frac{1}{p}\frac{R}{L_{S,c}}\frac{L_{z,c}}{L_{S,c}}i_{M,q} \\ &\quad - z\frac{\omega^2}{\omega^2+\left(\frac{1}{p}\frac{R}{L_{S,c}}\right)^2}\left(\frac{1}{2}\frac{L_{z,c}}{L_{S,c}}i_{M,d} + \frac{K_z}{L_{S,c}}\sqrt{\frac{3}{2}}\right) \\ i_{S,q} &= -z\frac{\omega^2}{\omega^2+\left(\frac{1}{p}\frac{R}{L_{S,c}}\right)^2}\frac{1}{2}\frac{L_{z,c}}{L_{S,c}}i_{M,q} \\ &\quad - z\frac{\omega}{\omega^2+\left(\frac{1}{p}\frac{R}{L_{S,c}}\right)^2}\frac{1}{p}\frac{R}{L_{S,c}}\left(\frac{1}{2}\frac{L_{z,c}}{L_{S,c}}i_{M,d} + \frac{K_z}{L_{S,c}}\sqrt{\frac{3}{2}}\right)\end{aligned} \tag{14}$$

where $L_{S,c} = L_c - M_c$ is the suspension synchronous inductance coefficient, defined for conciseness of the equations. The suspension current components depend linearly on the rotor axial position. Hence, as long as the rotor is centred, i.e. $z = 0$, there is no suspension current and therefore no electromagnetic force and torque related to the levitation, the self-bearing machine behaving as a conventional motor. In contrast, when the rotor is decentred, suspension currents are induced in the armature winding due to two distinct phenomena. On the one hand, as in the classical ironless structure, the rotor decentring leads to an unbalanced distribution of the permanent flux linked by the upper and lower windings and thus of the electromotive forces, resulting in the suspension current terms proportional to the flux gradient K_z. On the other hand, the difference between the upper and lower inductance coefficients $\mathbf{L_U}$ and $\mathbf{L_L}$ arising from their opposed evolution with the rotor axial position z creates an impedance imbalance between the windings, conducing to the suspension current terms proportional to the inductance variation $L_{z,c}$. As expected, the contribution linked to the direct-axis motor current $i_{M,d}$ adds to the one related to permanent flux linkage. It is also interesting to note that these additional current terms depend on the rate of axial variation of the inductance coefficients.

The total electromagnetic stiffness $k_{z,t}$ produced in quasi-static conditions can be obtained by substituting the current components (14) into (9) and (13):

$$k_{z,t} = -\frac{dF_{z,e} + dF_{z,r}}{dz} = \frac{\omega^2}{\omega^2 + \left(\frac{1}{p}\frac{R}{L_{S,c}}\right)^2} \times \underbrace{\left[\frac{3K_z^2}{L_{S,c}} + \frac{1}{2}\frac{L_{z,c}^2}{L_{S,c}}(i_{M,d}^2 + i_{M,q}^2) + 2K_z\frac{L_{z,c}}{L_{S,c}}\sqrt{\frac{3}{2}}\, i_{M,d}\right]}_{k_{z,t}^{\infty}} \tag{15}$$

The stiffness is independent from the rotor axial position but evolves with its spin speed ω, increasing until it reaches the asymptotic value $k_{z,t}^{\infty}$ for speeds far higher than the electrical pole. The first term of this asymptotic stiffness is identical to that acting in the ironless structure and thus corresponds to the classical electrodynamic restoring force, solely resulting from the flux linkage gradient K_z. The second term, that only involves the inductance coefficient variation $L_{z,c}$, corresponds to a reluctant force and is positive given its dependence to the square of both this parameter and the motor current norm. Consequently, both the quadrature-axis current $i_{M,q}$, controlled for the torque production, and the direct current component $i_{M,d}$, usually regulated to zero to prevent copper losses, lead to an increase of the total electromagnetic stiffness. The last term results from both the permanent flux linkage evolution K_z and the inductance coefficient variation $L_{z,c}$ with the rotor axial position. This cross contribution allows to modulate the total stiffness by improving or reducing its maximal value through the adaptation of the amplitude and the sign of the direct-axis motor current $i_{M,d}$. It should be noted that, in comparison with the equivalent ironless machine, both the flux gradient K_z and the synchronous suspension inductance coefficient $L_{S,c}$ of the structure under study is higher thanks to the additional rotor ferromagnetic yokes. This causes a diminution of the asymptotic stiffness $k_{z,t}^{\infty}$, on the one hand, but also of the electrical pole, implying that this asymptotic stiffness is reached at lower speeds.

The electrodynamic torque $T_{\alpha,e}$ can be evaluated in quasi-static conditions by introducing (14) into (10):

$$T_{\alpha,e} = p\sqrt{\frac{3}{2}}\left(K_\alpha - z^2\frac{\omega^2}{\omega^2 + \left(\frac{1}{p}\frac{R}{L_{S,c}}\right)^2}\frac{L_{z,c}}{L_{S,c}}K_z\right) i_{M,q} - z^2\frac{\omega}{\omega^2 + \left(\frac{1}{p}\frac{R}{L_{S,c}}\right)^2}\frac{R}{L_{S,c}}\left(\frac{3K_z^2}{L_{S,c}} + K_z\frac{L_{z,c}}{L_{S,c}}\sqrt{\frac{3}{2}}\, i_{M,d}\right) \tag{16}$$

In contrast with the ironless structure, the drive torque, produced through the quadrature-axis current $I_{M,q}$, has an additional component that depends on the square of the rotor

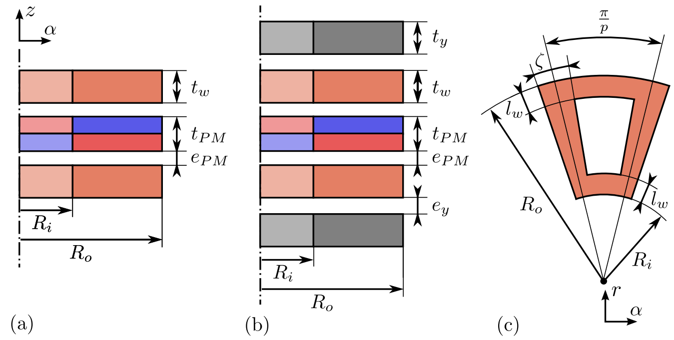

Fig. 2. Parametrisation of the self-bearing machine. (a) Ironless implementation. (b) Structure with rotor ferromagnetic yokes. (c) Winding.

axial position z and on the spin speed ω. Indeed, the permanent magnet flux linkage gradient K_z and the inductance coefficient variation $L_{z,c}$ being respectively positive and negative for the machine under study, the drive torque is enhanced by this cross term when the rotor is decentred. Moreover, the motor current does not only produce this torque but also contributes to the drag torque. Specifically, a cross term proportional to the direct-axis component $i_{M,d}$ also adds to the maximal value of the drag torque, leading to an increase or a reduction according to the sign of the current. Let us however remind that the drag torque peaks at the spin speed related to the electrical pole and then drops to zero at higher speeds.

IV. Case Study

This section aims at comparing the classical ironless implementation with the proposed structure comprising rotor ferromagnetic yokes based on the optimisation of existing motor and suspension performance metrics. The electromagnetic stiffness generated by two selected machines, including the additional terms resulting from the variation of the inductance coefficients with the rotor axial position, is then evaluated.

A. Performance Comparison

The performance comparison between both implementations relies on Pareto fronts resulting from a bi-objective optimisation performed on motor and suspension performance metrics through a NSGA-II algorithm.

1) Optimisation Parameters: As illustrated in Fig. 2, the structure with rotor ferromagnetic yokes is characterised through ten parameters among which four, namely the number of pole pairs p, the winding thickness h_w as well as the airgaps e_{PM} and e_y located on both sides of the windings, are determined via the optimisation process. The ironless implementation relies on identical parameters, except for

TABLE I
COMPARISON: FIXED DIMENSIONS

R_i	30 (mm)	t_y	3 (mm)
R_o	50 (mm)	t_{PM}	9.5 (mm)
ζ	$0.9\,\frac{\pi}{3p}$	l_w	$R_i\frac{\zeta}{1-\zeta}$

the second airgap e_y that does not apply. The remaining dimensions are fixed and summarised in Table I.

2) Optimisation Objectives: The optimisation is carried out based on motor and suspension performance metrics, denoted K_M and K_S, that have been derived for the ironless structure and therefore do not consider the impact of the inductance coefficient variation on the force and torque. They consist of the ratio of the axial restoring force and the motor torque to the square root of the underlying copper losses [16]:

$$K_M = \frac{T^M_{\alpha,e}}{\sqrt{P_M}} = pK_\alpha\sqrt{\frac{3}{R}}$$
$$K_S = \frac{F_{z,e}}{\sqrt{P_S}} = K_z\sqrt{\frac{3}{R}}\sqrt{\frac{\omega^2}{\omega^2 + \left(\frac{1}{p}\frac{R}{L_{S,c}}\right)^2}} \tag{17}$$

These metrics are independent from the number of loops, the motor and suspension currents as well as the rotor axial position z. Nevertheless, the suspension performance evolve with the spin speed ω. The flux constant K_α, flux gradient K_z and suspension synchronous inductance coefficient $L_{S,c}$ are identified through finite element simulations following the methods described in [11] while the electrical resistance R is calculated via Pouillet's law.

3) Optimisation Results: Fig. 3(a) depicts Pareto fronts resulting from a bi-objective optimization aiming at maximizing the motor K_M and suspension K_S performance metrics at a nominal rotor spin speed of 5000 (rpm) for the ironless and proposed rotors. As expected, the latter structure allows to reach significantly higher motor metric K_M for given suspension performance. Indeed, as shown in Fig. 3(b), the flux constant K_α is substantially improved due to the concentration of the permanent magnet flux achieved by the additional rotor ferromagnetic yokes. However, as represented in Fig. 3(c), this also causes the flux gradient K_z to decrease with respect to the ironless machine, directly impacting the axial restoring force. Despite this, the proposed rotor leads to slightly higher suspension metrics for low motor performance thanks to the increased inductance coefficients $L_{S,c}$ and therefore the reduced electrical pole, as illustrated in Fig. 3(d). The evolution of the winding thickness t_w with the suspension metric, presented in Fig. 3(e), is nearly identical for both machines. This implies that, due to the additional ferromagnetic yokes, the proposed structure has a larger total thickness than the ironless implementation. The increase of the winding thickness reduces the impact of the yokes on the permanent magnet flux linkage and, to a lesser extent, on the inductance coefficient. In addition, while the airgap e_{PM} between the magnets and the windings is constant and restricted by the optimisation lower bound, i.e. 1 (mm), the second airgap e_y between the windings and the yokes also expands along the Pareto front.

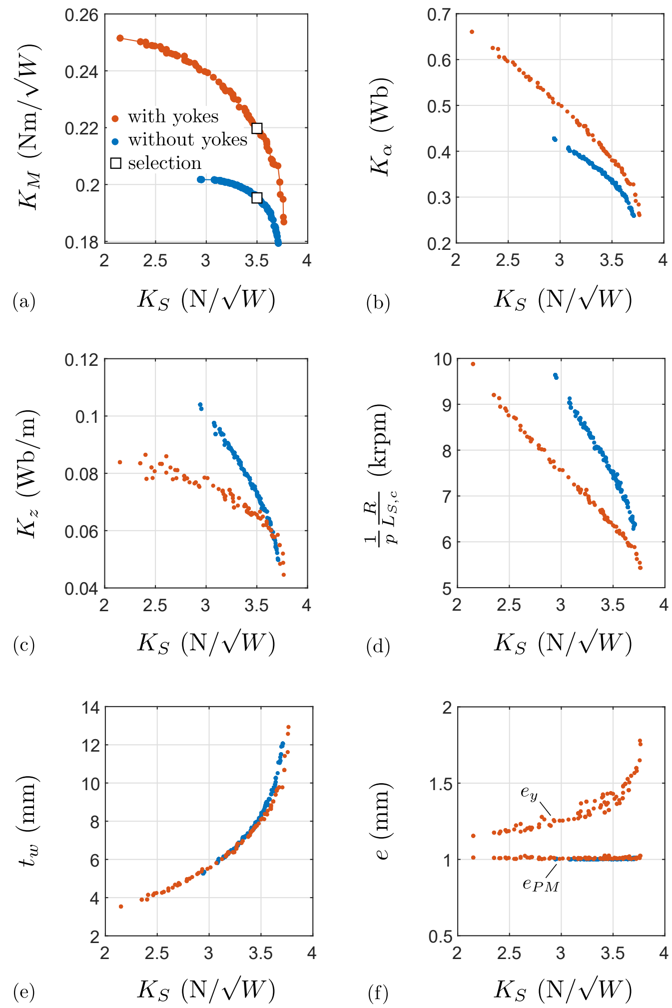

Fig. 3. Performance comparison between the classical ironless implementation and the proposed structure with ferromagnetic yokes. (a) Pareto fronts linking the motor and suspension performance metrics K_M and K_S. (b), (c), (d), (e) and (f) Evolution of the flux constant K_α, flux gradient K_z, electrical pole $R/(pL_{S,c}$, winding thickness t_w and airgap thickness along these fronts.

B. Quasi-static Analysis

Fig. 4 illustrates the evolution of the total electromagnetic stiffness $k_{z,t}$ with the rotor spin speed ω for the machines selected in Fig. 3(a). The solid and dashed lines correspond respectively to the ironless implementation and the proposed structure with rotor yokes when no motor current is supplied to the windings. Although both machines under comparison feature an identical suspension performance metric K_S, the former outperforms the latter in terms of stiffness in the complete speed range, also implying that it generates higher copper losses P_S so as to ensure the rotor axial levitation. According to the targeted application and, for instance, the possible compensation of predictable axial loads, the electromagnetic stiffness could directly constitute the suspension metric, considering that the rotor remains in its centred position in steady state and therefore generates no losses. In this case,

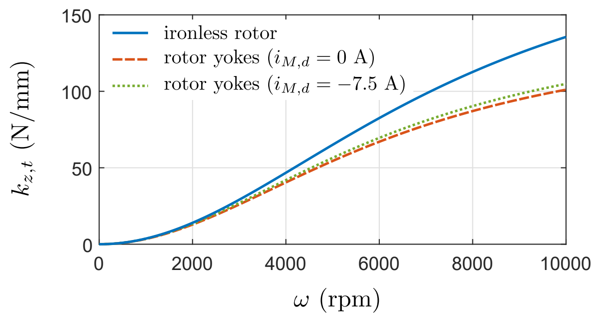

Fig. 4. Evolution of the total electromagnetic stiffness $k_{z,t}$ with the rotor spin speed ω for the classical ironless implementation and the proposed rotor structure with ferromagnetic yokes.

the results of the optimisations and thus the conclusion of the comparison might not be identical.

On the other hand, as stated in Section III-E, the injection of motor currents allows to benefit from the additional force terms resulting from the variation of the inductance coefficient with the axial position z. However, for the selected machine dimensions and a direct-axis motor current $I_{M,d}$ set to -7.5 (A), the reluctant stiffness is completely negligible while the cross term is small, amounting to only 3.7% of the electrodynamic one. Consequently, the impact on the total electromagnetic stiffness, represented by the dotted line, is limited. Note that the performance metrics based on which the comparison has been performed do not include the contribution to the force and torque production of these additional terms. Their importance, both in general and with respect to the classical electrodynamic term, has therefore not been maximised through the optimisation.

V. Conclusion

This paper proposes a rotor structure comprising ferromagnetic yokes surrounding the windings for axial flux passively levitated self-bearing machines. The existing electromechanical model is generalised so as to consider the resulting variation of the inductance coefficients with the axial position, highlighting that to the classical electrodynamic force are added reluctant and cross terms allowing to modulate the restoring stiffness and improve the drive torque through the motor current provided by the power supply.

The conventional ironless implementation and the proposed rotor structure are then compared in the framework of a case study, underlining that the additional ferromagnetic yokes allow to significantly improve the motor metric thanks to the permanent magnet concentration while slightly increasing the suspension performance. The quasi-static analysis underlines that, for machines with an identical suspension metric and in absence of motor current, the structure including yokes offers a lower electrodynamic stiffness than the ironless one but, in return, benefits from reduced underlying copper losses. On the other hand, taking into account that the additional force terms have not been optimised, the injection of direct-axis motor current has only a marginal impact on the total electromagnetic stiffness for the selected machine dimensions, the reluctant force contribution being completely negligible and the cross term only representing 3.7% of the electrodynamic stiffness.

Future works will include the derivation of motor and suspension performance metrics taking into consideration the additional force terms arising from the axial variation of the inductance coefficients and their use within an optimisation process to investigate the potential of the proposed structure.

References

[1] A. Chiba, T. Fukao, O. Ichikawa, M. Oshima, M. Takemoto, and D. G. Dorrell, *Magnetic bearings and bearingless drives*. Elsevier, 2005.

[2] W. Li, K. T. Chau, T. W. Ching, Y. Wang, and M. Chen, "Design of a high-speed superconducting bearingless machine for flywheel energy storage systems," *IEEE Transactions on Applied Superconductivity*, vol. 25, no. 3, pp. 1–4, June 2015.

[3] A. Tuysuz, T. Achtnich, C. Zwyssig, and J. Kolar, "A 300 000-r/min magnetically levitated reaction wheel demonstrator," *IEEE Transactions on Industrial Electronics*, vol. 66, no. 8, pp. 6404–6407, Aug. 2019.

[4] W. Bauer and W. Amrhein, "Electrical design considerations for a bearingless axial-force/torque motor," *IEEE Transactions on Industry Applications*, vol. 50, no. 4, pp. 2512–2522, July 2014.

[5] H. Sugimoto and A. Chiba, "Dynamic modeling and experimental validations of passing through critical speeds by high acceleration in one-axis actively positioned bearingless motors," *IEEE Transactions on Industry Applications*, vol. 57, no. 6, pp. 6956–6964, 2021.

[6] T. Reichert, T. Nussbaumer, and J. W. Kolar, "Bearingless 300-w pmsm for bioreactor mixing," *IEEE Transactions on Industrial Electronics*, vol. 59, no. 3, pp. 1376–1388, March 2012.

[7] D. Steinert, T. Nussbaumer, and J. W. Kolar, "Slotless bearingless disk drive for high-speed and high-purity applications," *IEEE Transactions on Industrial Electronics*, vol. 61, no. 11, pp. 5974–5986, Nov 2014.

[8] Y. Okada, N. Yamashiro, K. Ohmori, T. Masuzawa, T. Yamane, Y. Konishi, and S. Ueno, "Mixed flow artificial heart pump with axial self-bearing motor," *IEEE/ASME Transactions on Mechatronics*, vol. 10, no. 6, pp. 658–665, Dec 2005.

[9] N. Kurita, T. Ishikawa, N. Saito, T. Masuzawa, and D. L. Timms, "A double-sided stator type axial bearingless motor development for total artificial heart," *IEEE Transactions on Industry Applications*, vol. 55, no. 2, pp. 1516–1523, 2019.

[10] J. Chen, J. Zhu, and E. L. Severson, "Review of bearingless motor technology for significant power applications," *IEEE Transactions on Industry Applications*, vol. 56, no. 2, pp. 1377–1388, 2020.

[11] J. Van Verdeghem, M. Lefebvre, V. Kluyskens, and B. Dehez, "Dynamical modeling of passively levitated electrodynamic self-bearing machines," *IEEE Transaction on Industry Applications*, vol. 55, no. 2, pp. 1447–1460, March 2019.

[12] J. Van Verdeghem, V. Kluyskens, and B. Dehez, "Experimental investigations on passively levitated electrodynamic thrust self-bearing motors," *IEEE Transaction on Industry Applications*, vol. 55, no. 5, pp. 4743–4753, Sep. 2019.

[13] G. Cavalcante Rubio and A. Chiba, "Design and analysis of a bearingless motor with passive axial suspension through null-flux coils," in *2019 IEEE International Electric Machines Drives Conference (IEMDC)*, 2019, pp. 779–786.

[14] J. Van Verdeghem and B. Dehez, "Fully passively levitated self-bearing machine implemented within a reaction wheel," *IEEE Transactions on Industry Applications*, vol. 57, no. 6, pp. 5782–5795, 2021.

[15] G. C. Rubio, Y. Fujii, and A. Chiba, "A bearingless motor with passive electrodynamic suspension in axial direction," *IEEE Transactions on Industry Applications*, vol. 57, no. 6, pp. 6812–6822, 2021.

[16] J. Van Verdeghem and B. Dehez, "Performance comparison of wire-wound and pcb windings for passively levitated self-bearing machines," in *2021 24th International Conference on Electrical Machines and Systems (ICEMS)*, 2021, pp. 116–120.